



MODELING OF ELECTROMAGNETIC PROCESSES IN SHEATHS OF HIGH VOLTAGE CABLE LINES

Aleksander DYDYCZ ^{1*}, Kamil KIRAGA ²

¹Casimir Pulaski Radom University, Faculty of Transport and Electrical Engineering and Computer Science, Malczewskiego 29, 26-600 Radom, Poland, 114148@student.uthrad.pl

²Casimir Pulaski Radom University, Faculty of Transport and Electrical Engineering and Computer Science, Malczewskiego 29, 26-600 Radom, Poland, k.kiraga@uthrad.pl

DOI: <https://doi.org/10.24136/jaeec.2025.012>

Abstract – The paper presents a mathematical model of a three-phase high voltage cable line that accounts for wave phenomena and the influence of sheaths on current distribution and power losses. The model describes the time- and space-dependent behavior of current and voltage. The developed model uses the finite difference method to discretize the wave equations, enabling the analysis of changes in electrical parameters as functions of time and distance. Additionally, electromagnetic phenomena occurring in the return conductors of the cables are taken into account. A method for determining the induced currents in the return conductors, along with the calculated load current in the line, is used to present the waveforms of currents and voltages induced in the return conductors.

Keywords – high voltage lines, telegrapher's equations, sheath of high-voltage cables, currents induced, mathematical modeling.

INTRODUCTION

In an era of rapid development of power infrastructure, precise modeling and analysis of electromagnetic phenomena in high voltage transmission lines are becoming increasingly important. For lines with lengths comparable to the wavelength, the classical approach based on lumped parameter circuits proves insufficient. In such cases, it becomes necessary to account for wave phenomena and the time- and space-dependent relationships governing voltage and current waveforms. The fundamental analytical tool in this context is the telegrapher's equations, which enable the description of the dynamics of electrical signals in transmission lines with distributed parameters. A particular case that requires special attention involves high voltage cable lines, where additional phenomena arise due to the presence of return conductors. Currents induced in these conductors cause power losses and conductor overheating, which in turn limits their current-carrying capacity. The aim of this work is to present a mathematical

model of a three-phase high voltage cable line that includes wave phenomena, and to apply it to the modeling of processes occurring in the sheaths of the cables.

1 LITERATURE ANALYSIS

When a power line exceeds a certain length, it is considered as a circuit with distributed parameters. The electric charges moving through the conductors generate an electromagnetic field, which propagates at a specific, finite velocity described by the following formula [1, 2]:

$$v = \lambda * f \text{ [m/s]} \tag{1}$$

where: λ – wavelength [m]; f – frequency [Hz].

The propagation velocity determined from equation (1) may be less than or equal to the speed of light in a vacuum. Since an electromagnetic wave propagates at a finite speed, voltage and current signals also travel at a limited velocity. This means that the influence of current and voltage—for example, on a load located at a certain distance along a power line—will occur after a certain delay. If the length of the analyzed line is significantly shorter than the wavelength, a simplified approach may be used, treating the line as a lumped parameter circuit [3, 4]. In such a case, the line is assumed to be homogeneous, meaning its parameters are constant along its entire length. However, when the line length is comparable to the wavelength, it becomes necessary to use a distributed parameter model. For a line consisting of two conductors, small segments of length Δx , are analyzed, each characterized by unit parameters: resistance, inductance, conductance, and capacitance. These parameters are expressed per unit length—most commonly per meter or per kilometer [5, 6]. The schematic of the analyzed circuit is shown in Figure 1.

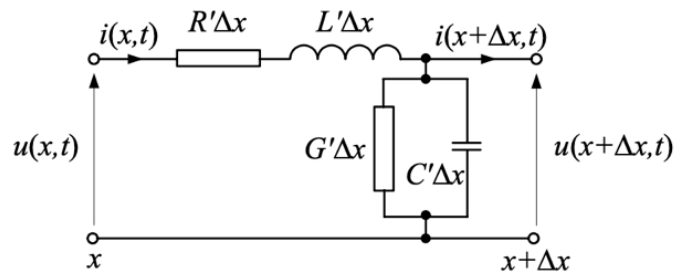


Fig. 1. Diagram of a two-wire line with distributed parameters [1]

Diagram shown in Figure 1 is described using voltage and current equations. After transforming these equations and taking the limit as the segment length Δx approaches zero, the telegrapher's equations are obtained:

$$\begin{aligned} -\frac{\partial u(x,t)}{\partial x} &= R * i(x,t) + L * \frac{\partial i(x,t)}{\partial t} \\ -\frac{\partial i(x,t)}{\partial x} &= G * u(x,t) + C * \frac{\partial u(x,t)}{\partial t} \end{aligned} \quad (2)$$

where: R, L, G, C – unit parameters: resistance, inductance, conductance, and capacitance.; u – voltage as a function of distance and time; i – current as a function of distance and time; x – distance; t – time. Equations (2) allow for the analysis of current and voltage waveforms as functions of time and distance from the beginning or end of the line [7, 8, 9].

The authors of publications [10, 11, 12] have developed precise models of long transmission lines based on differential equations that relate current and voltage as functions of both the distance from the beginning of the line and time. The high accuracy of electromagnetic phenomena modeling in phase conductors using the presented methods enables their further application in modeling secondary effects—for instance, in ground return circuits running parallel to the phase conductors.

Assuming that current and voltage have a constant angular frequency ω and a sinusoidal waveform, their RMS values can be expressed in complex form as:

$$\begin{aligned} \underline{U}(x) &= U(x) * e^{j\varphi_u(x)} \\ \underline{I}(x) &= I(x) * e^{j\varphi_i(x)} \end{aligned} \quad (3)$$

where: $\varphi_{u,i(x)}$ – are the phase angles of voltage and current, respectively.

In [1, 2] telegrapher's equations are presented as:

$$\begin{aligned} \frac{d^2 \underline{U}(x)}{dx^2} - \underline{\Gamma}^2 * \underline{U}(x) &= 0 \\ \frac{d^2 \underline{I}(x)}{dx^2} - \underline{\Gamma}^2 * \underline{I}(x) &= 0 \end{aligned} \quad (4)$$

Authors [1, 2] also provided solutions to these equations:

$$\begin{aligned} \underline{U}(x) &= \underline{U}_{1i} * e^{-\underline{\Gamma} * x} + \underline{U}_{1r} * e^{\underline{\Gamma} * x} \\ \underline{Z}_c \underline{I}(x) &= \underline{U}_{1i} * e^{-\underline{\Gamma} * x} - \underline{U}_{1r} * e^{\underline{\Gamma} * x} \end{aligned} \quad (5)$$

The quantities \underline{U}_{1i} and \underline{U}_{1r} in equations (5) represent the complex RMS values of the forward-traveling and reflected waves, respectively. The subscript 1 indicates that these values refer to the beginning of the line. The voltage at the beginning of the line $\underline{U}(0)$ is the sum of the incident and reflected waves. Based on equation (4), we get:

$$\begin{aligned} \underline{U}(0) &= \underline{U}_1 = \underline{U}_{1i} + \underline{U}_{1r} \\ \underline{Z}_c \underline{I}(0) &= \underline{Z}_c \underline{I}_1 = \underline{U}_{1i} - \underline{U}_{1r} \end{aligned} \quad (6)$$

From equations (5) and (6) we obtain:

$$\begin{aligned} \underline{U}(x) &= \frac{U_1 + Z_c I_1}{2} * (e^{-\Gamma * x} + n_1 * e^{\Gamma * x}) \\ \underline{I}(x) &= \frac{U_1 + Z_c I_1}{2 * Z_c} * (e^{-\Gamma * x} - n_1 * e^{\Gamma * x}) \end{aligned} \quad (7)$$

where n_1 is a reflection coefficient at the beginning of the line, dependent on the impedance on input and a characteristic impedance of the line. By transforming equation (7) using hyperbolic functions, we obtain [7]:

$$\begin{aligned} \underline{U}(x) &= \underline{U}_1 * \cosh(\underline{\Gamma} * x) - \underline{Z}_c * \underline{I}_1 * \sinh(\underline{\Gamma} * x) \\ \underline{Z}_c * \underline{I}(x) &= -\underline{U}_1 * \sinh(\underline{\Gamma} * x) + \underline{Z}_c * \underline{I}_1 * \cosh(\underline{\Gamma} * x) \end{aligned} \quad (8)$$

Equations (8) allow determination of the voltage and current at a point located in distance x from the beginning of the line, provided that the voltage and current at the start of the line are known [2].

In high voltage cable lines, additional power losses may occur due to currents induced in sheaths [13]. In configuration with sheaths connected and earthed on both sides (BE – both-ends), considering symmetrical load at the end of the line, current flowing in phase conductors causes current flow in sheaths. The phase currents and the sheaths currents are phase-shifted by 120° and 240° .

This configuration resembles a transformer with a short-circuited secondary winding, where the phase conductors act as the primary winding and the return conductors as the secondary winding [14, 15]. As a result of current flow through the return conductors, power losses occur across their resistances. In addition to power losses, the current flow causes heating of both the cable and the surrounding medium, leading to a reduction in the line's ampacity (current-carrying capacity). The calculation of induced current in the return conductors and the associated losses is performed using the concept of ground return circuits. The analyzed ground return circuits and their impedances in cable lines configured in triangular and flat arrangements are shown in Figure 2.

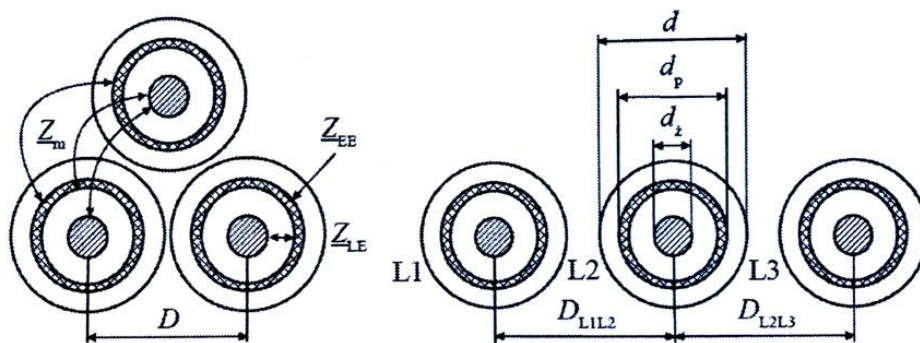


Fig. 2. Self and mutual impedances in cable lines [4]

In Figure 2, letters d , d_p and d_z denote the diameter of the cable, the diameter at the sheath, and the diameter of the main conductor respectively. The letter D represents distances between cable centers in cable line. Self-impedance of return wire is marked as Z_{EE} , and mutual impedance between the main wire and return wire is marked as Z_{LE} . The mutual impedance between ground return circuits is marked as Z_m . These notations are used in formula (9) which allows us to determine current induced in sheaths in both-ends structure [15, 16].

$$\frac{I_p}{I_z} = \frac{Z_{LE} - Z_m}{Z_{EE} - Z_m} = \frac{jX_p}{R_p + X_p}, \quad X_p = 0,145 * \lg\left(\frac{2 * D}{d_p}\right) \quad (9)$$

where: X_p – reactance per unit length of the return wire [Ω/km], R_p – resistance per unit length of the return wire [Ω/km], I_p – current in return wire [A], I_z – current in main wire [A].

When considering a single-point bonded (SPB) configuration, using the impedances from Figure 2 and Equation (9), the voltages induced in the return conductors can be calculated as follows [16]:

$$\begin{aligned} E_{p1} &= jI_z * 2 * \omega * 10^{-7} \\ &\quad * \left(-\frac{1}{2} * \ln\left(\frac{2 * D_{L1L2}^2}{d_p * D_{L1L3}}\right) + j\frac{\sqrt{3}}{2} * \ln\left(\frac{2 * D_{L1L3}}{d_p}\right) \right) \\ E_{p2} &= jI_z * 2 * \omega * 10^{-7} \\ &\quad * \left(\frac{1}{2} * \ln\left(\frac{4 * D_{L1L2} * D_{L2L3}}{d_p^2}\right) + j\frac{\sqrt{3}}{2} * \ln\left(\frac{D_{L2L3}}{D_{L1L2}}\right) \right) \\ E_{p3} &= jI_z * 2 * \omega * 10^{-7} \\ &\quad * \left(-\frac{1}{2} * \ln\left(\frac{2 * D_{L2L3}^2}{d_p * D_{L1L3}}\right) - j\frac{\sqrt{3}}{2} * \ln\left(\frac{2 * D_{L1L3}}{d_p}\right) \right) \end{aligned} \quad (10)$$

where: D_{LxLy} – distance between centers of specific cables [m].

2 MATHEMATICAL MODEL

Using wave equations (2) currents in the line were calculated at each spatial discretization step. The finite difference method was used. After transformation, the following formulas were derived for calculating current and voltage at the next time step:

$$\begin{aligned} i(m, n + 1) &= i(m, n) - \frac{dt}{L} \left(Ri(m, n) + \frac{u(m + 1, n) - u(m, n)}{dx} \right) \\ u(m, n + 1) &= u(m, n) \\ &\quad - \frac{dt}{C} \left(Gu(m, n) + \frac{i(m + 1, n) - i(m - 1, n + 1)}{dx} \right) \end{aligned} \quad (11)$$

where:

$$\frac{u(m+1, n) - u(m, n)}{dx} = \frac{du}{dx} \quad (12)$$

$$\frac{i(m, n+1) - i(m-1, n+1)}{dx} = \frac{di}{dx}$$

Letter m indicates the spatial step (where $dx=L/m$), and letter n indicates the time step (where $dt=dx/v$) and $v=1/\sqrt{LC}$ is the wave speed. Assuming a zero-impedance source, the current at the beginning equals the predicted next-step current: $i(1,t) = i(2,t)$.

For boundary conditions at the load, the voltage equals the voltage at the end of the line $u_l(n+1) = u(n)$ and the current is obtained from:

$$u_l(t) = R_l * i_l(t) + L_l * \frac{di_l(t)}{dt} \quad (13)$$

Value of $u_l(n+1)$ is known and equation (13) after discretization is:

$$i_l(n+1) = \frac{u_l(n+1) + L_l * \frac{i_l(n)}{dt}}{R_l + \frac{L_l}{dt}} \quad (14)$$

Then, knowing the current at the end of the line, the influence of the main conductor current on sheaths is calculated using equations (9) and (10).

3 COMPUTER SIMULATION RESULTS

A cable line composed of three cables was considered, with the phase conductor made of aluminum and the return conductor made of copper. The cable insulation was made of XLPE material. The construction parameters of the cables are presented in Table 1.

Table 1. Construction parameters of single 110 kV cable.

Conductor cross section	Conductor diameter	Insulation diameter	Sheath cross section	Diameter on sheath	Cable diameter
mm ²	mm	mm	mm ²	mm	mm
1000	38	68.6	95	74.4	84

Calculations were performed for a flat arrangement with the distance between the cable axes equal to twice their diameter. The per-unit-length parameters of the cable line (in the flat arrangement), determined based on the construction data, are as follows: $R_0 = 3.6232 \cdot 10^{-5} \Omega/m$, $L_0 = 5.3212 \cdot 10^{-7} H/m$, $C_0 = 2.3544 \cdot 10^{-10} F/m$, $G_0 = 2.9587 \cdot 10^{-12} S/m$. The phase voltage applied was defined by the function $u = 64 * \sin(\omega t)$ kV. The line was terminated with a resistive-inductive

load with the following parameters: $R = 250 \Omega$, $L = 1 \text{ H}$. In the first calculation case, a 20 km long line in a flat conductor arrangement was analyzed. Figure 3 shows the voltage waveforms along the line at times $t=0.00019 \text{ s}$ and $t=0.015 \text{ s}$. It is clearly visible that at $t=0.00019 \text{ s}$ electromagnetic wave has not yet reached the end of the line. At $t=0.015 \text{ s}$ the voltage distribution along the line is nearly flat, due to the relatively short line length.

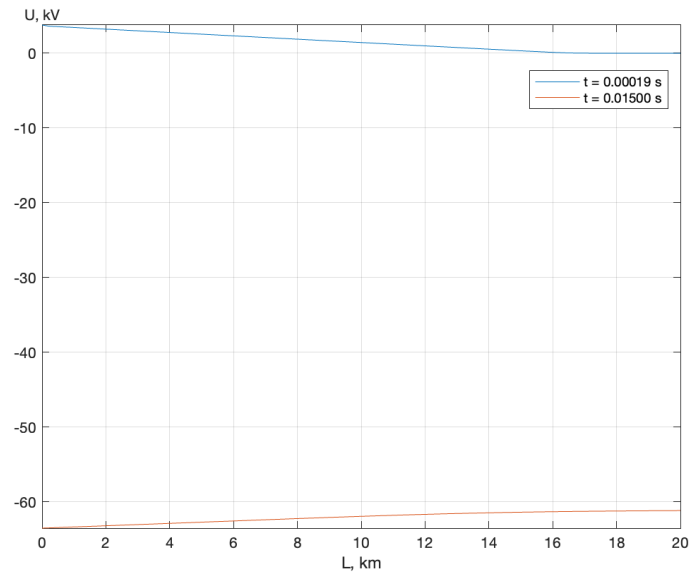


Fig. 3. Voltage distribution along a 20 km line at times $t=0.00019 \text{ s}$ and $t=0.015 \text{ s}$.

Figure 4 presents the current waveform at the end of the 20 km line. Different colors represent the current waveforms for each phase: blue for phase L1, red for L2, and yellow for L3. Initial current distortions are clearly visible, which fade out as the steady state is reached at around $t = 0.09 \text{ s}$. The initial current reaches a maximum value of about 174 A in phase L1, whereas in steady state, the current in all three phases equals 157 A.

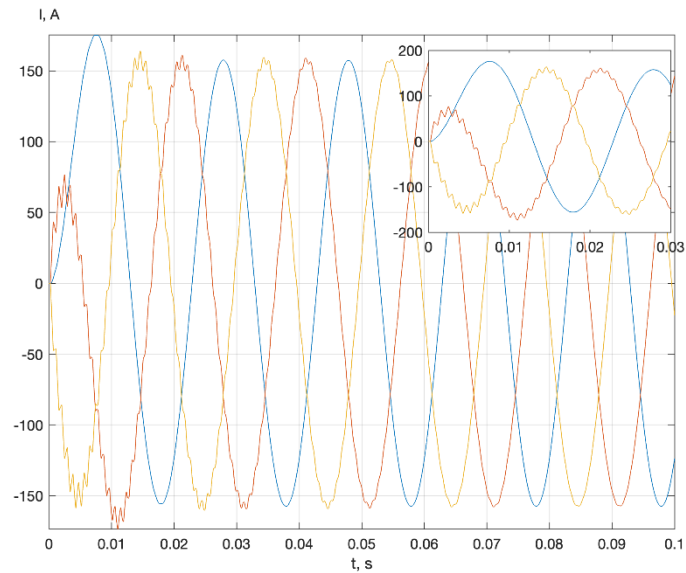


Fig. 4. Current waveform at the end of the 20 km line.

Using the determined current in the phase conductors of the HV line, the current induced in the return wires was calculated. Figure 5 shows the waveform of the induced current in the return conductors at the midpoint of the line.

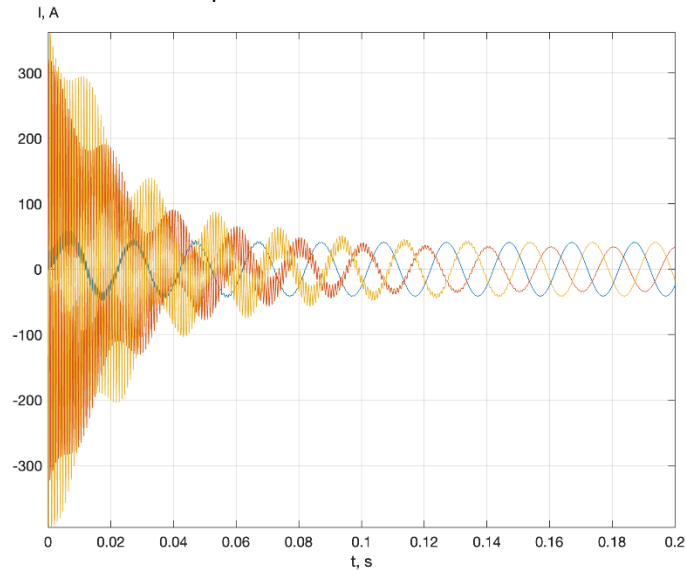


Fig. 5. Current waveform in the sheaths at the midpoint of the 20 km line.

The waveforms shown in Figure 5 for phases L2 and L3 may indicate instability in the numerical method used to solve the differential equations. Since we are analyzing the line

in a flat arrangement, the induced currents in the return conductors are not identical. The asymmetrical positioning of the cables causes a lower induced current in phase L2. In steady state, the current in phases L1 and L3 is about 41 A, while in phase L2 it is approximately 34 A.

Assuming a single-point grounding configuration for the return conductors eliminates the closed ground-return loop of the return conductors. The absence of grounding at one end of the line results in the induction of electromotive force in the return conductors. The highest electromotive force value appears at the ungrounded end of the line.

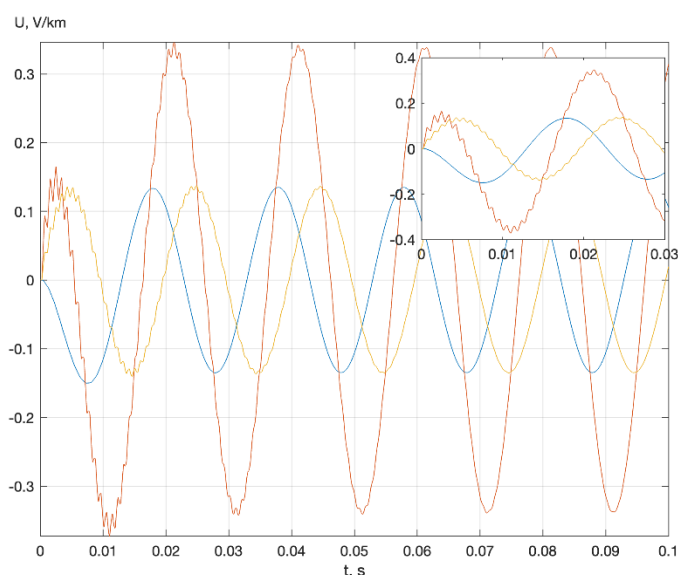


Fig. 6. Induced electromotive force waveform in the return conductors at the end of the 20 km line.

Figure 6 shows the EMF waveform induced at the ungrounded end of the return conductors. Since in the flat arrangement the impedances of the center and outer lines differ, the voltage induced in the return conductor of the center cable is more than twice as high as that in the return conductors of the outer cables. The voltage induced by the load currents is about 0.33 V/km in the return conductor of the center cable and about 0.14 V/km in the return conductors of the outer cables. It should be noted that in the case of transient states or faults, the values of the induced electromotive forces may increase significantly.

4 CONCLUSIONS

The presented model, based on the telegrapher's equations, allows for highly accurate determination of the operating parameters of the line. The distorted current waveforms shown in the study at the end of the line do not differ significantly from the steady-state waveforms, as the assumed cable line length is only 20 km. The peak current value during the transient state is only about 10% higher than the value in the steady state.

The use of a line model employing the telegrapher's equations makes it possible to accurately determine the current and voltage induced in the cable sheaths, depending on the adopted grounding configuration. Knowing the precise values of currents and voltages in the return conductors enables the correct selection of protection equipment and allows assessment of the impact of the grounding arrangement on the transmission capacity and operational parameters of the line. Analyzing the mathematical model allows prediction of system behavior and helps replace part of the empirical testing, which leads to reduced costs and complexity of real-world experiments.

BIBLIOGRAPHY

- [1] Piątek Z., Jabłoński P. (2017) „Podstawy teorii pola elektromagnetycznego”. Warszawa, Wydawnictwo Naukowe PWN SA
- [2] Konane D., Ouedraogo W., Guingane T., Zongo A., Koalaga Z., Zougmore F. (2022) “An Exact Solution of Telegraph Equations for Voltage Monitoring of Electrical Transmission Line”. *Energy and Power Engineering*. Vol. 14, No. 11, pp 669-679, doi: 10.4236/epe.2022.1411036
- [3] Lopez-Fernandez X. M., Alvarez-Marino C., Malo-Machado Vitor. (2010) “Computation Method for Transients in Underground Cables With Lossy Earth Return Path”. *Magnetics, IEEE Transactions* Vol. 46, No 8, pp 2911 – 2914, doi: 10.1109/TMAG.2010.2043074
- [4] Żmuda K. (2016) „Elektroenergetyczne układy przesyłowe i rozdzielcze. Wybrane zagadnienia z przykładami”. Gliwice, Wydawnictwo Politechniki Śląskiej
- [5] Lis M., Chaban A., Szafraniec A., Levoniuk V., Figura R. (2019) “Mathematical modeling of transient electromagnetic processes in a power grid”. *Przegląd Elektrotechniczny*. Vol 12/2019 R. 95, pp 160-163, doi: 10.15199/48.2019.12.35
- [6] Jakubowski J., Cichy A., Rakowska A. (2023) „Wytyczne projektowania linii kablowych 110kV”. Poznań, Polskie Towarzystwo Przesyłu i Rozdziału Energii Elektrycznej
- [7] Haddad D., Kallel A. Y., Essoukri ben Amara N., Kanoun O. (2021) “Modeling Reflections in a Complex Cable Structure with Impedance Mismatches”. *Conference International Workshop on Impedance Spectroscopy (IWIS)*, doi: 10.1109/IWIS54661.2021.9711910
- [8] Jin W., Wang D., Gao H., Peng F., Guo Y., Gao M., Wang J. (2024) “Two-terminal traveling wave fault location approach based on frequency dependent electrical parameters of HVAC cable transmission lines”. *Electric Power Systems Research*, Vol. 235, No 110842, doi: 10.1016/j.epsr.2024.110842
- [9] Chaban A, Popena A, Perzyński T, Szafraniec A, Levoniuk V. (2024) “Mathematical Model of a Nonlinear Electromagnetic Circuit Based on the Modified Hamilton–Ostrogradsky Principle”. *Energies*. Vol 17(21):5365. <https://doi.org/10.3390/en17215365>
- [10] Chaban A., Popena A., Szafraniec A., Levoniuk V. (2023) “Including shield wires in the analysis of transient processes occurring in HVAC transmission lines”. *Energies*. Vol 16(23), Issue 7870, doi: 10.3390/en16237870
- [11] Chaban A., Lis M., Szafraniec A., Levoniuk V. (2022) “Mathematical modelling of transient processes in a three phase electric power system for a single phase short-circuit”. *Energies*. Vol 15(3), Issue 1126, doi: 10.3390/en15031126

-
- [12] Chaban A., Lis M., Szafraniec A., Levoniuk V., Chaban A. (2022) „Analiza procesów nieustalonych w trójfazowej długiej linii zasilania z asymetrycznym obciążeniem”. *Przegląd Elektrotechniczny*. Vol 12/2022 R. 98, pp 209-212, doi: 10.15199/48.2022.12.47
- [13] Duda D., Szadkowski M. (2014) „Ochrona przeciwprzepięciowa osłon kabli WN w różnych układach połączeń żył powrotnych”. *Przegląd Elektrotechniczny*. Vol. 10/2014, R. 90, pp 37-40, doi: 10.12915/pe.2014.10.09
- [14] Duda D., Szadkowski M. „Kable ECC w układzie SPB kabli wysokiego napięcia”. *Przegląd Elektrotechniczny*. Vol 10/2016, R. 92, pp 104-107, doi: 10.15199/48.2016.10.25
- [15] Łowczowski K. (2016) „Badanie wpływu ułożenia kabli na straty energii w żyłce powrotnej – symulacja w programie PowerFactory”. *Przegląd Elektrotechniczny*. Vol. 10/2016, R. 92, pp 54-57, doi: 10.15199/48.2016.10.13
- [16] Czapp S., Dobrzyński K., Klucznik J., Lubośny Z. (2017) „Analiza napięć indukowanych w żyłkach powrotnych kabli wysokiego napięcia dla ich wybranych konfiguracji”. *Zeszyty Naukowe Wydziału Elektrotechniki i Automatyki Politechniki Gdańskiej*. Vol 53/2017, pp 83-86

